Theory of Polymer Adsorption and Colloid Stabilization in Supercritical Fluids. 2. Copolymer and End-Grafted Stabilizers

J. Carson Meredith and Keith P. Johnston*

Department of Chemical Engineering, University of Texas at Austin, Austin, Texas 78712

Received February 19, 1998; Revised Manuscript Received May 26, 1998

ABSTRACT: The interaction of two planar surfaces coated with polymeric steric stabilizers is described as a function of polymer conformation with lattice-fluid self-consistent field theory. For block copolymer stabilizers, as the solvent density and thus solvent quality are lowered, expansion of the stabilizer block due to excluded volume interactions associated with an increase in adsorption competes with collapse due to a loss in stabilizer solubility. In contrast, grafted chains only collapse as solvent density is lowered. The effects of changing anchor and stabilizer solubility, block lengths, and anchor adsorption energy are explored. For two surfaces coated with either adsorbed copolymer or grafted stabilizers, free energies of interaction are calculated and used to identify the critical flocculation density (CFD). The CFD occurs very close to the upper critical solution density (UCSD) for the same molecular weight stabilizer tail in bulk solution. This correspondence between a surface property (CFD) and a bulk property (UCSD) is in agreement with stability experiments in supercritical CO_2. Based on the free energy calculations, we identify design criteria for effective end-grafted and copolymer stabilizers.

Introduction

In part 1 of this series[1] we examined homopolymer adsorption, layer structure, and steric stabilization at the solid−supercritical fluid interface. Here we consider end-grafted stabilizers and diblock copolymers consisting of a rather insoluble anchor block that adsorbs strongly to an impermeable surface, and a nonadsorbing stabilizer block that is preferentially solvated. Adsorption of copolymers from a *selective* solvent is a common approach to achieve steric stabilization of latexes and emulsions.[2] Copolymers containing highly CO_2-soluble poly(1,1-dihydroperfluorooctyl acrylate) (PFOA) appear promising as steric stabilizers to prevent flocculation of particles.[3,4] Turbidimetry[5] and dynamic light scattering[6] experiments along with measurements of copolymer adsorption have been utilized to determine the mechanism of stabilization of poly(ethylhexyl acrylate) emulsions with polystyrene(PS)-*b*-PFOA in liquid and supercritical CO_2. The PS-*b*-PFOA also stabilizes poly(methyl methacrylate) (PMMA) and PS particles produced by precipitation with a compressed fluid antisolvent.[7] Copolymers with poly(propylene oxide) (PPO) and poly(butylene oxide) (PBO) tails can also stabilize PMMA particles in CO_2.[8] Recently, the mechanism of the dispersion polymerization of PMMA in CO_2 was studied in situ for a grafted poly(dimethyl siloxane) (PDMS) stabilizer.[9,10]

For liquid solvents, Marques et al.[11] presented a theory of diblock copolymer adsorption from a selective solvent to a planar impermeable surface. Their theory describes successfully the variation of adsorbed amount with chain architecture in liquid solvents.[12] This theory might adequately describe the adsorption of copolymers from a supercritical solvent at high, liquidlike densities. However, because solvent is not included explicitly, the theory of Marques et al. will not be applicable as solvent density is decreased and solvent compressibility becomes more important.

Polymers end-grafted to a surface represent a convenient boundary condition for diblock copolymer adsorption, because the grafted amount remains constant as solvent quality is varied. End-grafted polymers consist of a highly soluble stabilizer tail bound irreversibly to the surface, usually with a chemically reactive end segment. Szliefer[13] and Grest[14] reviewed the theory and simulation of end-grafted layers in incompressible solvents. To treat grafted chains in a compressible solvent, the theory must model the free volume of the solvent. To do this, Peck[15] originally developed the lattice-fluid self-consistent field (LFSCF) theory and modeled short ($r = 50$) grafted polymer layers in subcritical solvents near the lower critical solution temperature (LCST).

Our objective is to understand the effect of solvent quality on the structure of adsorbed and grafted layers and on the interaction of two surfaces coated with such layers in a compressible solvent. We use LFSCF theory, in which holes are added to the lattice to include solvent compressibility. The next section presents a brief discussion of the LFSCF theory and the selection of parameters for this study. Results for grafted chains are presented as a basis for the more complicated behavior of adsorbing copolymers. In particular we show how the layer thickness depends on grafted amount and solvent density, which controls stabilizer solubility. The free energy of interaction of surfaces with grafted polymers is calculated and used to identify the onset of flocculation at the critical flocculation density (CFD). For copolymers, adsorption, layer structure, and the free energy of interaction are examined as a function of copolymer structure (asymmetry), anchor and stabilizer solubility, copolymer concentration, and anchor adsorption energy. The results are compared with experimental results where possible. Conformational changes of grafted and adsorbed polymers and the CFD are related to the phase behavior in bulk solution. A theoretical foundation is provided for understanding the correlation between the CFD and phase behavior of the stabilizer tails in bulk solution, which has been observed in experiments in supercritical CO_2.[5,6] By systematically examining the effect of stabilizer architecture, solubility, and adsorption affinity on the CFD, design criteria are developed for grafted and copolymer stabilizers.

S0024-9297(98)00260-5 CCC: $15.00
Published on Web 07/28/1998

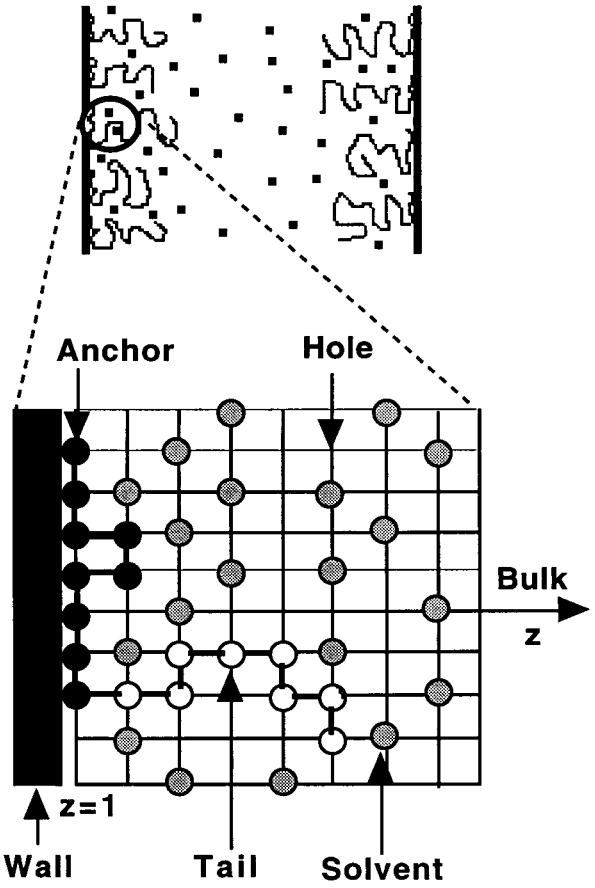

Figure 1. Schematic of the lattice-fluid self-consistent field theory.

Theory

LFSCF Theory. The LFSCF theory was originally developed for homopolymers by combining incompressible self-consistent field (SCF) theory[16,17] with the lattice-fluid (LF) equation of state.[18,19] Here the LFSCF theory is generalized to treat copolymer structure in the manner of Evers et al.,[20] who adapted the incompressible SCF theory[17] to model copolymer adsorption. Figure 1 presents a schematic showing how copolymers, containing anchor (A) and stabilizer (B) segments, solvent (s), and holes (o) are modeled with a lattice. The surfaces are immersed in a solution containing copolymer. The details relevant to the extension of LFSCF theory to copolymers are in the Appendix. Our code was verified by reproducing results of incompressible SCF theory[16,17] and LFSCF for end-grafted chains.[15] The adsorbed amount, layer thickness, free energy of interaction, and Hamaker interaction between surfaces are calculated as in part 1 of this series.[1]

Parameters. In LFSCF theory, as in the LF equation of state[19] for bulk solutions, each segment type requires three parameters: r_i, the segments per molecule or block, P_i^*, the segment cohesive energy density, and v^*, the segment volume. For simplicity, v^* is the same for all components. The solvent parameters, are discussed in part 1 of this series.[1] All calculations are performed at $T_r = T/T_c = 1.05$, where $T_c = 319$ K, the critical temperature of the model solvent. The density range is $0.7 < \tilde{\rho} < 1$, or $1.4 < \tilde{\rho}/\tilde{\rho}_c < 2$, where $\tilde{\rho}_c$, the solvent critical density, is 0.5. The actual experimental density range of CO_2 at $T_r = 1.05$ (45 °C) is $1.1 < \rho/\rho_c < 1.9$ over the pressure range of 100 to 300 bar. Thus, the theory covers the range of pressure and density relevant to the experiments.

Table 1. Copolymer Parameters and Comparison to Polymer Surface Free Energies

system	ν_A	P_A^* (atm)	P_B^* (atm)	ϵ_{AW} (kT)	P_A^*/P_B^*
LFSCF	0.25	2300	1600	3.0	1.44
	0.03−0.67	2300	1200	3.0	1.92
	0.25	2300	1000	3.0	2.30
	0.25	1900	1600	3.0	1.19
	0.03−0.67	1900	1200	3.0	1.58
	0.25	1900	1000	0.5, 1.0, 3.0	1.90
	0.25	1500	1200	3.0	1.25
expt.		PS	PFOA	3.4−5.7[a]	1.7−2.0[c]
		PVAc	PFOA	5.9[b]	1.9[c]
		PS	PDMS	3.4−5.7[a]	1.2−1.4[c]

Note: The total chain length ($r_A + r_B$) is 300 segments. [a] Styrene adsorption onto activated carbon from CO_2 at 45 °C (ref 48). [b] Poly(vinyl acetate) adsorption onto silica from CCl_4 at 25 °C (ref 49). [c] $P_A^*/P_B^* \propto (\gamma_A/\gamma_B)^{0.5}$, where γ_A is the experimentally determined polymer surface free energy, (ref 22).

Table 1 gives copolymer chain parameters used in this work, along with a few properties of copolymers typically used in experiments in CO_2 for comparison. The total number of segments in the copolymer is $r_A + r_B = 300$ in all cases, representing a molecular weight of 15 000 to 30 000, depending on the segmental molecular weight. The fraction of anchor segments, ν_A, is varied over a wide range.

The P_A^* and P_B^* values control the magnitude of inter- and intrasegmental interactions, and hence determine the compatibility of solvent and polymer. The three P_A^* values of 2300, 1900, and 1500 atm, examine anchor blocks which are incompatible ($\chi_{AS} = 0.5$), somewhat compatible ($\chi_{AS} = 0.26$), and quite compatible ($\chi_{AS} = 0.095$) at $\tilde{\rho} = 1$. The incompatibility increases substantially as $\tilde{\rho}$ is decreased starting from 1, so the χ_{AS} values already presented represent the maximum anchor compatibility at the incompressible limit. The P_B^* values of 1000 ($\chi_{BS} = 0$ at $\tilde{\rho} = 1$), 1200 ($\chi_{BS} = 0.017$), and 1600 ($\chi_{BS} = 0.13$) model a range of stabilizer cohesive energy densities (CED) close to and above that of the solvent, as is encountered in actual experiments. At a $\tilde{\rho}$ of 0.85, the effective values of χ_{BS} increase to 0.146, 0.188, and 0.371, respectively. The ratio P_A^*/P_B^* is proportional to $\sqrt{\gamma_A/\gamma_B}$, where γ_i is the polymer surface free energy, a property closely related to CED.[21,22] Because PFOA is highly soluble in CO_2, we chose $P_B^* = 1000 = P_S^*$. Given this basis and the experimental values of γ_i, $P_{PDMS}^* \approx 1400$ and $P_{PPO}^* \approx 1700$ atm. Table 1 also shows that the model P_A^*/P_B^* ratios are similar to those for copolymers used in experiments in CO_2.

The segmental adsorption energy, ϵ_{AW}, describes the energy gained when one anchor segment is adsorbed and is 3 kT in most cases. Above ~3 kT, ϵ_{AW} has little effect on the adsorption or stability results; many common anchor groups can be modeled with ϵ_{AW} values of 1−5 kT.[17,23] Experimental adsorption energies for styrene adsorption onto activated carbon in CO_2 at 45 °C are 3.4−5.7 kT over a range of solvent densities.

In a selective solvent, copolymers can form self-assembled structures such as spherical and lamellar micelles.[24] In the presence of an adsorbing surface, there exists a complicated equilibrium between free chains, micelles, and adsorbed chains. The competition between micelle formation and adsorption of free chains is driven by low anchor segment solubility (favoring

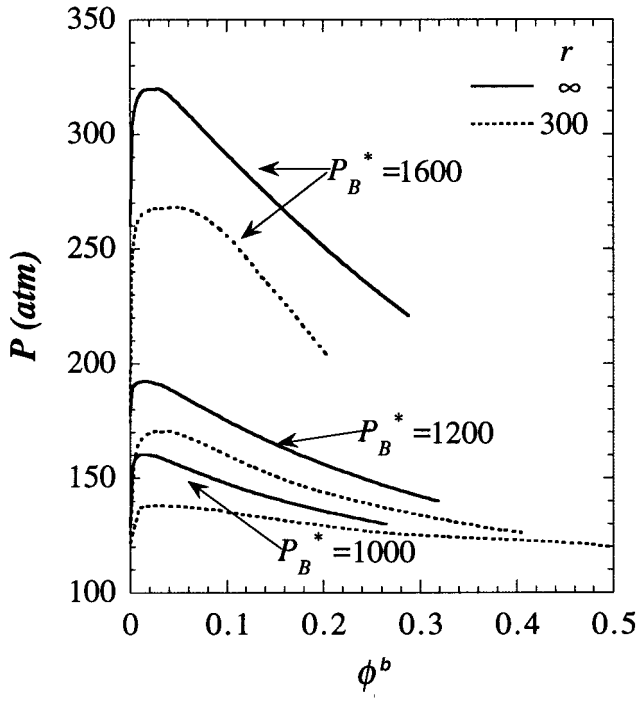

Figure 2. P (atm)$-\phi^b$ (polymer volume fraction) phase diagram for stabilizer at $T = 336$ K ($T_r = 1.05$) and $P_B^* = 1000$, 1200, and 1600 atm (cohesive energy density of tail) for $r = 300$ and $r = \infty$. The solvent critical density, $\tilde{\rho}_c$, is 0.5 and has CO_2-like parameters given in the text.

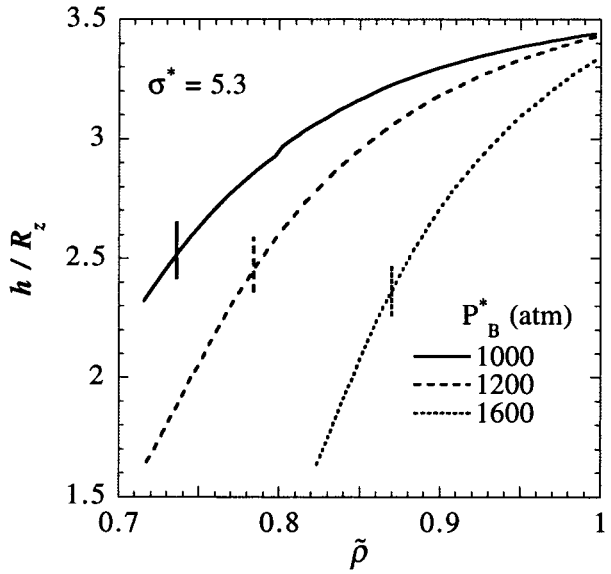

Figure 3. Layer thickness normalized to z-component of bulk end-to-end distance, h/R_z (good solvent), versus solvent bulk density, $\tilde{\rho}$, at $P_B^* = 1000$, 1200, and 1600 atm (cohesive energy density). The chains are grafted with grafting density $\sigma^* = 5.3$. The vertical marks indicate upper critical solution densities in bulk solution.

micelle formation) and high adsorption energy (favoring adsorption). In addition polymer−solvent incompatibility occurs as the solvent quality is reduced, which ultimately leads to the formation of polymer-rich and polymer-lean phases (e.g., UCST and LCST type phase separation). It is beyond the scope of this work to consider equilibrium between all four of these phases simultaneously. Rather we are interested in the effect of solvent density when soluble nonmicellar free chains adsorb to a surface. The bulk copolymer volume fraction is $\phi^b = 10^{-4}$, which is well within the one phase region at all pressures used in this work. We found that adsorbed amounts and layer structure are relatively insensitive to changes in concentration, over the volume fraction range $10^{-7}-10^{-2}$ for $\epsilon_{AW} = 3\ kT$, as is also observed in many experiments of strong copolymer adsorption from selective solvents.[12] To favor adsorption over micelle formation, the theory of Munch et al.[25] gives an estimated minimum ϵ_{AW} of 0.13 to 0.29 kT for the range of anchor P_A^* used in this work. The adsorption energies in this work, shown in Table 1, are above these minimum values.

Results and Discussion

Polymer−Solvent Phase Behavior. Figure 2 shows the pressure−composition bulk phase diagram of the solvent and stabilizers examined in this paper. The binodal phase boundaries were obtained with the lattice-fluid theory.[26] Three P_B^* values are examined: 1000 atm, identical to the solvent, and 1200 and 1600 atm. For each P_B^* value, the phase boundaries for both $r_B = 300$ and $r_B = \infty$ are presented. As pressure is lowered at constant temperature, a phase boundary occurs where the solution separates into high-density (polymer-rich) and lower-density (solvent-rich) phases. This phase separation is driven by the large free volume difference between polymer and solvent, which grows larger as density is reduced. By expanding away from the chain into a lower density phase, the solvent gains enough entropy to overcome the loss in entropy of mixing and loss of chain−solvent and solvent−solvent attractive interactions. This pressure−composition diagram is analogous to the well-known LCST, or thermally induced phase separation of polymer solutions.[18,27] For each r_B and P_B^* value there is a critical pressure where phase separation is first possible (Table 2). In the limit of $r_B = \infty$, the critical pressure is equal to the Θ pressure, P_Θ, where the binary attractive and repulsive interactions of a chain are balanced (Table 2).

Table 2. Critical Pressures and Densities of Stabilizer Tail−Solvent Solutions

	$r_B = \infty$		$r_B = 300$	
P_B^* (atm)	P_Θ (atm)	$\tilde{\rho}_\Theta$	critical pressure (atm)	UCSD
1600	320	0.871	268	0.859
1200	192	0.784	170	0.770
1000	160	0.737	146	0.722

Grafted Chains. Figure 3 shows how layer thickness changes with bulk solution density for brushes composed of end-grafted chains. The grafted layer is exposed to pure solvent at $T_r = 1.05$, and because $\sigma^* = 5.3$, the layer is in the overlapping regime, which starts at $\sigma^* = 1$. The layer thickness, h (eq 2), is normalized with R_z, the z-component of the bulk root mean square (rms) end-to-end distance of the stabilizer chain in the good solvent (swollen) limit. The value of R_z is taken as one-third of the end-to-end distance obtained from Flory's theory.[28] For a single ideal grafted chain (second virial coefficient is zero), $h/R_z = 2$.[29] The chain is stretched relative to bulk dimensions, due to volume excluded by the surface. At high $\tilde{\rho}$, $h/R_z > 2$ because the chains are swollen with solvent and because of excluded volume from chain−chain overlap. As $\tilde{\rho}$ is decreased, the chains collapse toward the surface as the solvent expands into the bulk solution. The nonadsorb-

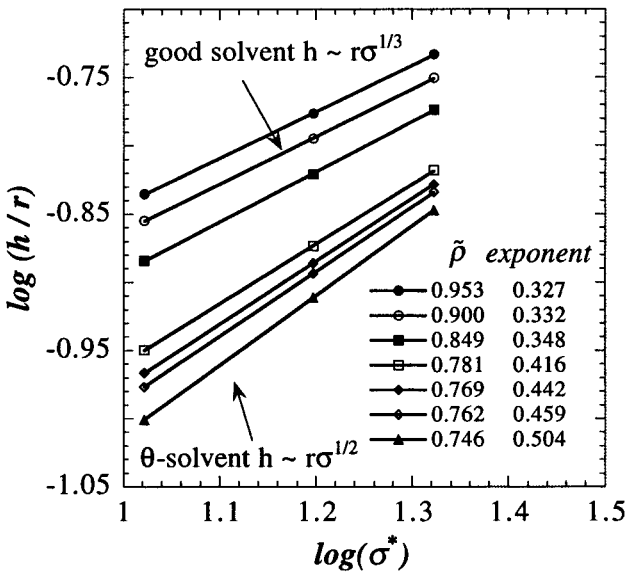

Figure 4. A test of the good and Θ-solvent scaling of layer thickness with respect to graft density: log(h/r) versus log(σ^*). The exponent is the slope, x, of the best fit line, where $h/r \sim (\sigma^*)^x$.

ing segments do not interact with the surface, rather, the chain collapses because less solvent is present to screen the intra- and intersegmental interactions. As P_B^* is raised further away from that of the solvent (1000 atm), solubility decreases and the collapse occurs at higher densities, in correspondence with the bulk phase diagram, where $\tilde{\rho}_\Theta$ increases with P_B^*. The Θ density in bulk solution is marked by vertical lines. For all P_B^* values in Figure 3, the grafted layers are collapsed by ~30% at $\tilde{\rho}_\Theta$, relative to the thickness at $\tilde{\rho} = 1$.

Because grafted chains are constrained by attachment to the surface they cannot phase separate in the usual sense for bulk solutions. As solvent density is decreased, the grafted chains collapse, causing an increase in chain concentration within the grafted layer. Thermodynamic instability occurs when the concentration rises to the critical value at the critical solution density for a bulk solution. Thus the curves in all figures end at this instability density. This instability was verified with the lattice fluid equation of state[19] by calculating the spinodal stability curve for chains in bulk solution at the concentration of stabilizer in the outermost region of the layer (not shown).[19] The LFSCF equations cannot be solved below the instability density unless modified to include the presence of another surface (i.e., flocculation) or lateral phase separation (i.e., 2-dimensional SCF). The interactions between two surfaces will be considered later in this paper, but the consideration of lateral phase separation is beyond the scope of this study. Recent publications have treated lateral phase separation of brushes induced by changes in solvent quality,[13,30,31] although these studies did not consider supercritical solvents.

In the overlapping, strong stretching regime, classical scaling[32,33] and analytical SCF[34,35] theories predict that $h \sim r\sigma^x$, where $x = 1/3$ and $1/2$ in the good and Θ-solvent regimes, respectively. These predictions have been verified with simulations,[30] analytical SCF,[35] and mean field theory[13] of grafted brushes near a UCST, where energetic differences between solvent and chain drive phase separation. These relations have not been tested

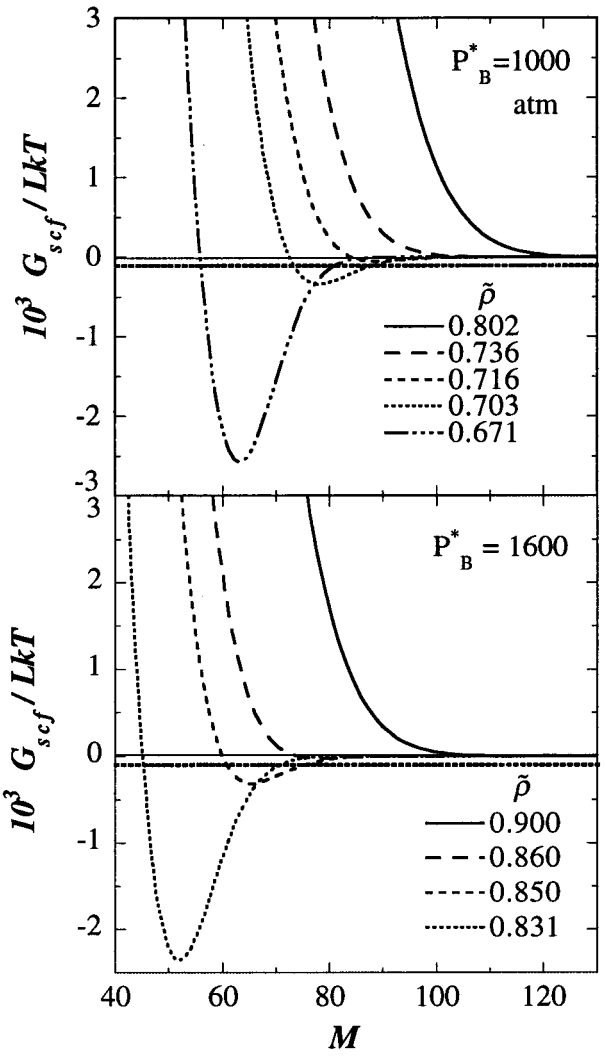

Figure 5. Free energy of interaction of grafted polymers, $\Delta G/LkT$, versus distance of separation of bare surfaces, M, for $P_B^* = 1000$ and 1600 atm (cohesive energy density) at $T_r = 1.05$ and $\sigma^* = 5.3$ (grafting density). The horizontile dotted line denotes the flocculation threshold energy.

for grafted layers near a LCST, where solvent entropy drives changes in chain conformation.

We present in Figure 4 a test of the good and Θ scaling regimes with respect to grafting density, σ, over the range $5 < \sigma^* < 25$ for $r = 300$. At high densities ($0.85 < \tilde{\rho} < 0.99$) the scaling of $h/r \sim \sigma^{1/3}$ in a good solvent agrees with the LFSCF results. As $\tilde{\rho}$ is decreased, there is a monotonic increase in the scaling exponent from 1/3 to 1/2. The Θ solvent scaling occurs just below $\tilde{\rho}_\Theta = 0.784$, at $\tilde{\rho}$ ~0.75, which is the density of pure solvent at the critical pressure of the 300 segment chains in bulk solution. The classical Θ point scaling law just presented will occur exactly at $\tilde{\rho}_\Theta$ only in the limit of a strongly stretched brush ($\sigma^* \sim 10^2$ and $r = \infty$). Thus, the agreement between classical scaling and LFSCF theory indicates that chains adopt swollen and ideal dimensions in good and Θ solvents, respectively, regardless of whether solvent strength is determined by energetics (near an UCST) or by entropy (near a LCST).

In Figure 5 the free energy of interaction per unit area, $\Delta G/LkT$, is shown for two planar surfaces coated with end-grafted polymers at a grafting density of $\sigma = 0.01$, or $\sigma^* = 5.3$. The surfaces are immersed in a bath

of pure solvent, in equilibrium with the space between the surfaces. The interactions between surfaces are repulsive at solvent densities above the UCSD of the stabilizer chains in bulk solution. Repulsion arises primarily from the loss in entropy due to overlap of the grafted layers. The repulsive wall moves to smaller M values as solvent density decreases due to the collapse of the grafted layer, seen in Figure 3. This repulsion first appears when the polymer layers begin to overlap, according to the volume fraction profiles (not shown). As density is decreased below the bulk solution UCSD, negative values of $\Delta G/LkT$ indicate attraction. The strength of the attraction grows rapidly with density. The attraction arises from the increase in solvent entropy as it expands into the lower density bulk region.[15] In analogy with LCST phase separation in bulk polymer solutions, the solvent entropy gain offsets the repulsion caused by overlapping of chains. At very close distances, repulsion again dominates. The Hamaker interaction between model PS particles were calculated in part 1[1] and the layers in Figures 5a and b are thick enough to screen the Hamaker interaction at all densities.

A key issue is the relation between polymer phase behavior in bulk solutions and the CFD of the polymer-coated surfaces. The negative free energy necessary for flocculation, ΔG_{floc}, may be estimated by considering the kinetic energy of a colloidal particle due to Brownian motion. This kinetic energy is, on average, 3/2 kT per particle. The effective area of contact upon collision, L, must be known, because the free energies in Figure 5 are plotted per unit area. From the Langbein approximation[36] for large spherical interacting particles, we obtain $L \approx 10^4$ lattice units for a 500-nm particle, which yields $\Delta G_{floc}/LkT \approx -10^{-4}$. At $P_B^* = 1000$ atm, where solvent and chain have symmetric energetic interactions, similar to the value for PFOA, this flocculation energy is achieved at a CFD = 0.71, which is just 0.012 below the UCSD for chains of length $r_B = 300$ in bulk solution. At $P_B^* = 1600$, qualitatively similar to the value for PDMS and PPO, the CFD occurs just below the UCSD of 0.857. As the mismatch between chain and solvent P^* increases, attraction occurs at higher densities, in correspondence with the phase diagram for stabilizer blocks in bulk solutions (Figure 2). The CFD always occurs just below the UCSD, but moves toward the UCSD as P_B^* increases. At higher P_B^*, the onset of attraction also occurs at closer distances because the layers are more collapsed (Figure 3).

Copolymers: Adsorption and Conformation. Adsorption of diblock copolymers from a selective solvent is often modeled as a thin wetting layer of anchor segments covering most of the surface and a layer of overlapping stabilizer tails that extend into the solution. In Figure 6 volume fraction profiles for adsorbed copolymer show that the thin anchor layer occupies ~2−4 lattice layers (8−17 Å) and covers ~95% of the surface. Due to the high A−B incompatibility, the stabilizer layer is depleted at the surface and the tails extend ~50 lattice layers (220 Å) into the solution. The tails are stretched relative to thebulk dimensions of the stabilizer in a good solvent, where the end-to-end distance is 27 lattice units. The volume fraction of the stabilizer brush falls off to the bulk solvent concentration ($\phi^b = 10^{-4}$) with an exponential form. The shape of the stabilizer profile in Figure 6 is similar to that

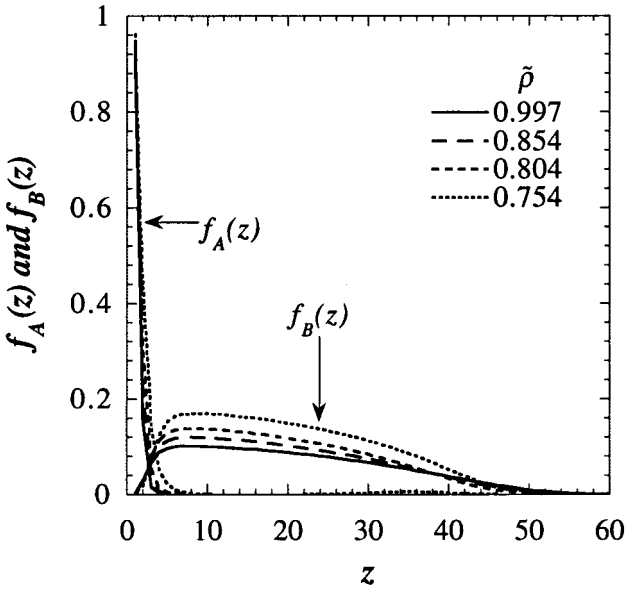

Figure 6. Volume fraction profiles of anchor [$f_A(z)$] and stabilizer [$f_B(z)$] segments at several bulk densities for $P_A^* = 2300$ atm, $P_B^* = 1200$ atm (cohesive energy density), $\nu_A = 0.25$ (anchor fraction), $\epsilon_{AW} = 3.0\ kT$ (adsorption energy), and $\phi^b = 10^{-4}$ (concentration).

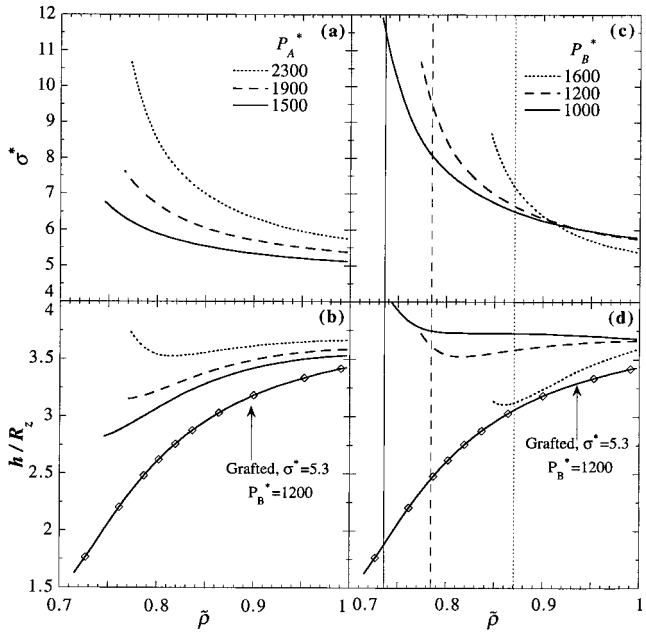

Figure 7. Normalized adsorbed amount (σ^*) and layer thickness (h/R_z) versus reduced bulk density, $\tilde{\rho}$, for various copolymers with $\nu_A = 0.25$ (anchor fraction) at $T_r = 1.05$. Unless indicated otherwise, $\epsilon_{AW} = 3.0\ kT$ and $\phi^b = 10^{-4}$. (a), (b): $P_B^* = 1200$ atm. Effect of varying P_A^* (anchor cohesive energy density) is shown. (c), (d): $P_A^* = 1900$ atm. Effect of varying P_B^* (tail cohesive energy density) is shown.

observed in neutron scattering experiments[37,38] in liquids and in computer simulation.[30,39] As bulk solvent density decreases, the stabilizer segment fraction increases somewhat, indicating an increase in adsorbed amount, but the outer region of stabilizer tails collapses slightly, reflecting the diminishing solubility of the tails.

Figure 7a presents the response of adsorption to the anchor segment cohesive energy density (solubility), P_A^*. The σ^* values fall between 5 and 12, which is a typical range in experiments in liquid solvents.[40]

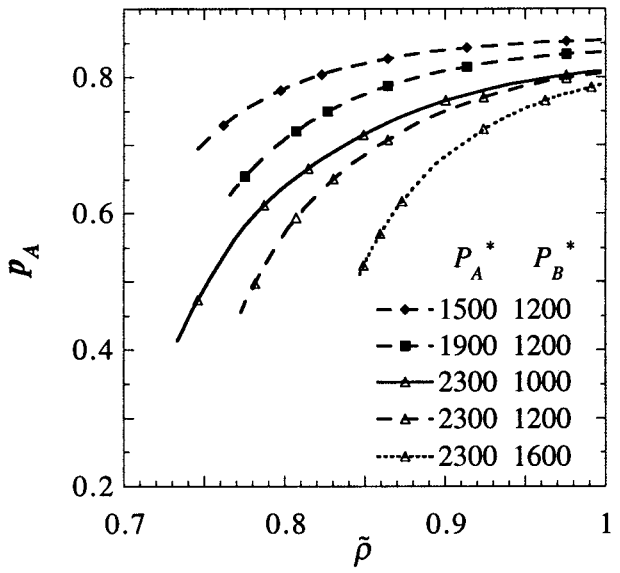

Figure 8. Bound fraction of anchor segments, p_A, versus bulk solution density for various P_A^* and P_B^* (cohesive energy density) with $\epsilon_{AW} = 3.0\ kT$ (adsorption energy) and $\phi^b = 10^{-4}$.

Adsorption measurements in CO_2 yield $\sigma^* = 3.6$ for a PS−PDMS block copolymer ($M_w = 2000-16000$) adsorbed on a PS surface at $T_r = 1.05$, $P = 238$ bar, and $\phi^b \approx 10^{-5}$.[41] Because $\sigma^* > 1$, the stabilizer tails overlap and stretch normal to the surface, but the layer cannot be considered a true "brush", where σ^* is typically >50.[40] In Figure 7a, σ^* increases monotonically with a decrease in bulk solvent density, $\tilde{\rho}$, because the decrease in bulk solvent quality drives more chains to adsorb to the surface. As P_A^* is increased, the anchor and solvent become more incompatible and the σ^* curves shift upward. Figure 8 indicates that the fraction of total anchor segments adsorbed to the surface, p_A, decreases as $\tilde{\rho}$ decreases and as P_A^* increases. Thus, some adsorbed anchor segments desorb to create space and allow more chains to add to the surface and escape the increasingly incompatible solvent. The percentage of the surface covered with adsorbed anchor blocks (not shown) is between 88 and 98%, and increases only slightly with increasing P_A^*. Thus, the "lift-off " of anchor segments occurs at approximately constant surface coverage.

Figure 7b shows a comparison of the layer thickness of adsorbed and grafted chains, where the bulk chain end-to-end distance, R_z, is 31.7 lattice units in a good solvent. As the bulk solution density is decreased, the adsorbed layer does not collapse as much as the grafted layer, because chains continue to add to the surface. For the same reason, the chains collapse less as P_A^* is increased. In fact, at $P_A^* = 2300$ atm, a minimum in h is observed at $\tilde{\rho} \sim 0.81$, which is very close to the copolymer UCSD in bulk solution of 0.817. As density is lowered, the collapse-to-expansion transition reflects the competition between increasing adsorption (causing expansion) and stabilizer insolubility (causing collapse). This transition is also observed with adsorbing homopolymers,[1] but not with end-grafted stabilizers at a fixed graft density.

Consider the effect of changing the stabilizer CED, P_B^*, for a constant P_A^* of 2300 atm. In Figure 7c, the σ^* curves shift to higher density as P_B^* increases, reflecting the increase in stabilizer insolubility. For this reason, σ^* shifts to about the same extent as $\tilde{\rho}_\Theta$ for the stabilizer block (indicated by vertical lines in Figure 7c). Figure 8 indicates that the bound fraction of anchor segments, p_A, decreases at all densities as P_B^* increases (Figure 7d). Just as with increasing P_A^*, the system sacrifices a few adsorbed segments to allow more chains to add. Changes in P_B^* directly affect the layer extension of the stabilizer block into the solvent, whereas changes in P_A^* primarily influence the adsorption, which affects the layer thickness indirectly. Figure 7d indicates that the optimum stabilizer studied, for which layer collapse is minimized, has a CED equal to that of the solvent. With copolymers (unlike homopolymers) there is flexibility in adjusting the layer thickness and location of the collapse-to-expansion transition, because anchor and stabilizer solubility can be changed independently. For example, increasing P_A^* and decreasing P_B^* enhance layer thickness as solvent density is decreased, due to increased adsorption, provided that ϵ_{AW} remains sufficiently high. In experiments, the P_A^* and ϵ_{AW} can rarely be changed independently, and significant increases in P_A^* can decrease affinity for the surface because of mismatch of anchor and surface CED.[42]

The adsorption energy per anchor segment influences whether adsorption or depletion of surfactant chains occurs. At low $\epsilon_{AW} = 0.5\ kT$, σ^* is close to zero and a depletion layer is formed (not shown). When ϵ_{AW} is increased to $1\ kT$, adsorption occurs, and at $\epsilon_{AW} \geq 3\ kT$, the segments become strongly bound to the surface and further increases in ϵ_{AW} have little effect, as observed in other SCF studies as well.[17] Because our anchor blocks tend to be rather short relative to stabilizer blocks (25% anchor in Figure 7), segmental adsorption energies of several kT are required to achieve significant adsorption. This results is in contrast to long homopolymers containing thousands of segments,[1,43] where rather weak segmental adsorption energies, $<1\ kT$, can provide strong adsorption of chains. The reason for our choice of a small fraction of anchor segments will become apparent in the free energy of interaction section.

Figures 6−8 consider only one copolymer structure, with $r_A + r_B = 300$ and 25% anchor segments. The fraction of anchors per chain, ν_A, can be used to adjust the response of layer structure to changes in $\tilde{\rho}$. At each density in Figure 9a there is an optimum $\nu_A(\max)$, where a maximum in σ^* occurs. This optimum occurs between 0.07 and 0.1 over the density range of $0.77 < \tilde{\rho} < 0.997$. When ν_A is decreased below $\nu_A(\max)$, there are too few anchors to balance the entropic penalty for adsorbing a chain, and the adsorbed amount decreases. When $\nu_A > \nu_A(\max)$, the surface becomes crowded with anchors and surface coverage reaches a plateau value of $\Theta_A \approx 0.95$ (Figure 9b). The adsorbed amount responds to the crowding of anchor segments at the surface in two different ways. At high density ($\tilde{\rho} = 0.997$), σ^* decreases monotonically as ν_A increases above $\nu_A(\max)$. This behavior is observed in adsorption experiments[12] and SCF theory[16] in liquid solvents. However, at low solvent density below the copolymer UCSD, σ^* decreases with increasing ν_A because of anchor crowding, until a local minimum is reached at $\nu_A(\min)$, and then σ^* begins to increase again. The increase in σ^* when ν_A is well above $\nu_A(\max)$ occurs at approximately constant surface coverage (Figure 9b). As discussed with Figures 7 and 8, at densities just below

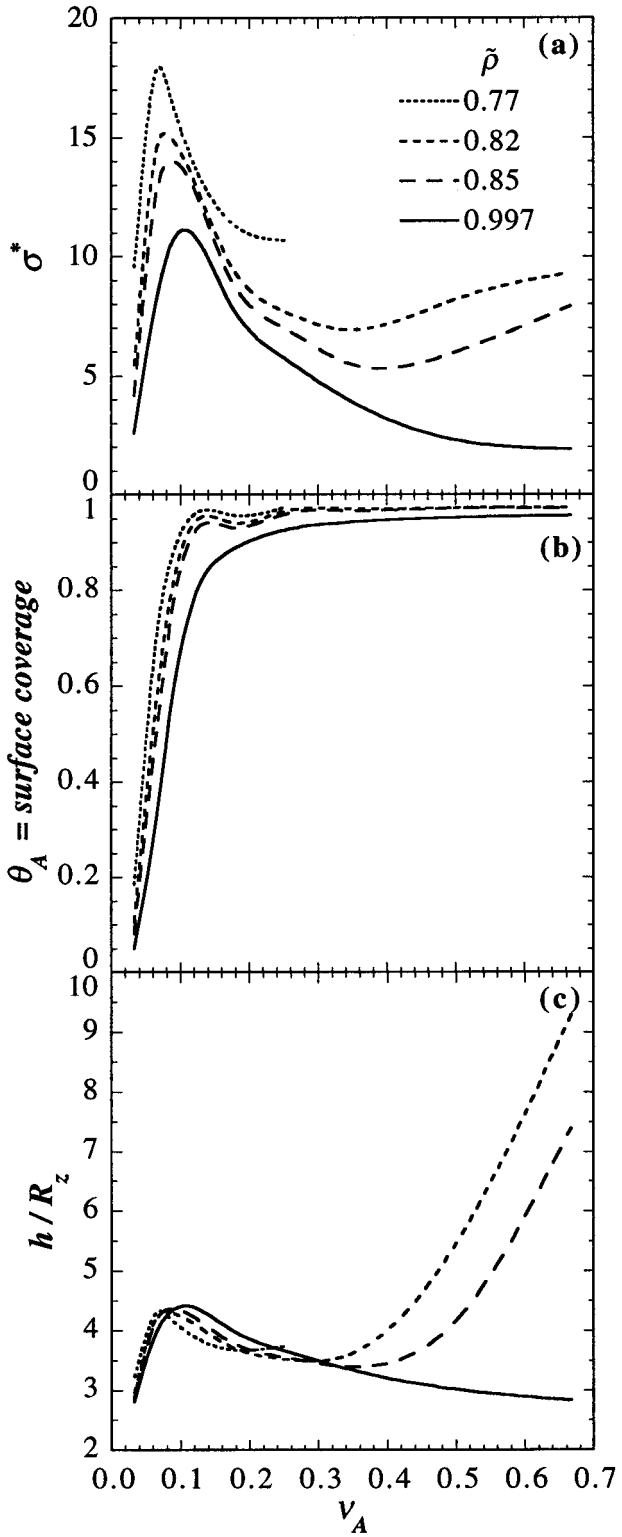

Figure 9. Adsorbed amounts (σ^*), surface coverage by anchor segments (Θ_A), and layer thickness (h/R_z) versus anchor fraction (ν_A) for a total chain length of $r = 300$. Other chain properties are $P_A^* = 2300$, $P_B^* = 1200$ (cohesive energy density), $\epsilon_{AW} = 3.0\ kT$ (adsorption energy), and $\phi^b = 10^{-4}$.

the *copolymer* UCSD in bulk solvent, some adsorbed anchor segments "lift-off" the surface to allow new surfactant to escape the poor bulk solvent by adsorbing to the surface. Similarly, the copolymer also becomes insoluble as the fraction of anchor increases at constant density, leading to increased adsorption and the "lift-off" effect when $\nu_A > \nu_A(\text{min})$. The "lift-off" effect was also observed in LFSCF calculations of adsorbed homopolymers.[1]

Table 3. Scaling Exponents (x) from $\sigma^* \sim \beta^x$ at Various Densities ($P_A^* = 2300$, $P_B^* = 1200$, $\phi^b = 10^{-4}$, $\epsilon_{AW} = 3$ kT)

$\tilde{\rho}$	x
0.997	0.96
0.90	0.80
0.85	0.70
0.82	0.69
0.80	0.64

Figure 9c demonstrates that ν_A has a profound effect on the response of layer thickness to decreasing solvent density. Maxima and minima in h/R_z occur near the maxima and minima in σ^*, respectively. One may divide Figure 9c into a regime of layer collapse as density is decreased, due to the anchor−solvent incompatibility, and layer expansion, as chains adsorb to escape the poor solvent conditions. The same collapse-to-expansion transition occurs in Figures 7b,d. In fact, Figure 9c demonstrates that a chain with 50% anchor segments at low density can have a much larger layer thickness than a chain with 20 % anchor segments at high density. As a note of caution, our treatment neglects the formation of micelles or of a condensed polymer-rich phase, which would reduce the supply of free copolymer available for adsorption.

The dependence of σ^* on chain asymmetry may be understood more clearly by considering the relationship between σ^* and the chain asymmetry parameter, $\beta = (r_B)^{6/5}/(r_A)^{2/3}$. The parameter β indicates the ratio of the projected areas of the swollen tail to the collapsed anchor.[11] For liquid solvents, when σ^* is relatively insensitive to changes in bulk polymer concentration, as in our LFSCF calculations and in many experiments,[12] σ^* is predicted to scale with β according to $\sigma^* \propto \beta^{18/23} \approx \beta^{0.78}$. Parsonage et al.[44] show that for $10 < \beta < 100$, this scaling law is obeyed for poly(vinylpyridine)-*b*-PS and poly(vinylpyridine)-*b*-poly(isoprene) copolymers adsorbed onto silica and mica from toluene solutions at 25 °C. Table 3 indicates the scaling exponents, x, when the LFSCF results of Figure 9a are fit to σ^* versus β^x. At $\tilde{\rho} = 0.90$ the scaling exponent ($x = 0.8$) is close to the predicted liquid solvent value ($x = 0.78$). At this high density, the supercritical solvent behaves like a liquid solvent, and the LFSCF theory yields the same scaling exponent as from experiments in liquid solvents.[44] As $\tilde{\rho}$ decreases, x decreases continuously. As the solvent quality becomes poorer for the stabilizer tails, the good solvent scaling exponent for stabilizer ($r_B^{6/5}$) is no longer applicable, and the Marques scaling law fails.

Copolymers. Free energy of interaction. In Figure 10, the free energy of interaction, $\Delta G/LkT$, is shown versus separation distance, M, for two copolymers, with P_A^* and P_B^* chosen to model PS−PFOA (Figure 10a) and PS−PDMS (Figure 10b). In Figure 10a, $P_B^* = 1200$ atm, and $\nu_A = \nu_A(\text{max}) = 0.083$. At high density, the free energy is repulsive, but ΔG becomes negative near $\tilde{\rho} = 0.776$. The minimum in ΔG continues to grow as $\tilde{\rho}$ is lowered and reaches the flocculation threshold at 0.764, the CFD. The flocculation threshold in $\Delta G/LkT$ was already defined as -10^{-4} for a 500-nm particle. The minimum in ΔG at the CFD occurs at $M = 130$ lattice layers, which is far outside the effective range of the Hamaker interaction energy of the bare surfaces, indicating Hamaker forces will not

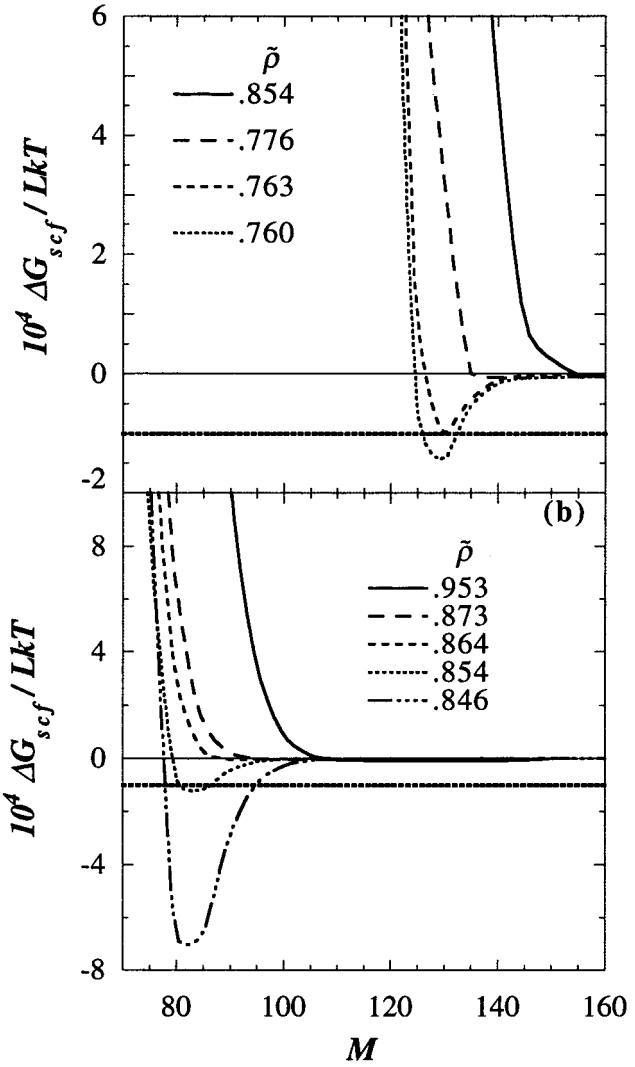

Figure 10. $10^4\,\Delta G/LkT$ versus plate separation, M, at various bulk densities for $r = 300$, $\epsilon_{AW} = 3.0\ kT$, and $\phi^b = 10^{-4}$. The horizontal dotted lines represent the free energy minimum necessary for flocculation of two surfaces under Brownian motion: (a) $P_A^* = 2300$, $P_B^* = 1200$, and $\nu_A = 0.0833$; (b) $P_A^* = 2300$, $P_B^* = 1600$, and $\nu_A = 0.25$ (anchor fraction).

cause flocculation. In Figure 10b, where $P_B^* = 1600$ atm and $\nu_A = 0.25$, the CFD is 0.854, and the ΔG minimum occurs at $M = 85$ because the stabilizer is shorter and more incompatible with the solvent than in Figure 10a. However, the Hamaker interaction energy is still effectively screened by the chains. The values of CFD in Figures 10a and b are essentially equal to the UCSDs for the stabilizer tails in bulk solution, which occur at densities of 0.768 and 0.854, respectively.

Table 4 lists the calculated stabilizer tail UCSD and the surfactant CFD as a function of block copolymer architecture, solubility, adsorption energy, and concentration. The LFSCF calculations predict flocculation, very close to the critical point of the phase boundary (UCSD) for many of the cases considered. For the stabilizer tail lengths considered, the UCSD is always lower than the Θ-density at infinite molecular weight, as shown in Table 2. To examine the effect of chain properties on stabilization, Table 4 is grouped into sets in which one property is varied while others are held constant. The CFD is presented for surfaces coated with surfactant, both with and without the Hamaker interaction between the surfaces. Without Hamaker attraction, the surfaces flocculate at the stabilizer UCSD in most cases. When the adsorbed or grafted layer is of sufficient thickness, adding the Hamaker attraction changes the CFD negligibly. However, if the layer is not thick enough to screen the Hamaker interaction, the CFD occurs above the UCSD. In this case, flocculation occurs due to Hamaker attraction before the onset of LCST phase separation. For example, the grafted chain CFDs in set 1 correspond closely to the UCSDs for $r_B = 300$. When r_B is decreased to 100, the Hamaker attraction overwhelms steric repulsion and flocculation occurs at all densities.

Concentration. Set 2 indicates that concentration has no observable effect on CFD over the range 10^{-5}–10^{-6} and the chain with the same ν_A and P_B^* in set 4 has the same CFD even at $\phi^b = 10^{-4}$. Over this concentration range, the supply of chains is sufficient to guarantee good surface coverages for these strong adsorption energies.

Anchor Fraction. In set 3, decreasing the anchor fraction from 0.083 (close to ν_A(max)) to 0.017 causes the CFD to increase and become significantly larger than the UCSD. The decreasing adsorption and layer thickness (Figure 9a) may allow the Hamaker force to cause attraction before LCST-type attraction occurs. As ν_A is decreased further to zero, the chains will not adsorb and flocculation is inevitable. Set 4 indicates the effect of increasing ν_A above ν_A(max). The CFD corresponds to the UCSD until ν_A increases above 0.5, where the CFD increases above the UCSD, again due to decreased adsorption and layer thickness. At the highest anchor fraction, 0.67, there are *two* regions of flocculation. Attraction occurs when $\tilde{\rho} > 0.85$ because the layer thickness is inadequate to screen the Hamaker forces. As density is decreased below 0.85, the surfaces are stabilized as adsorbed amount and layer thickness increase significantly due to the "lift-off" effect, and the Hamaker forces are screened. When $\tilde{\rho} < 0.77$, Hamaker and LCST attraction cause flocculation. In contrast, surfaces coated with grafted chains with $r_B = 100$ and the same initial surface coverage (set 1) flocculate at *all* densities, due to Hamaker forces, because grafted amount does not increase as density is decreased.

Adsorption Energy. The CFD changes negligibly with adsorption energy between 6 and 0.8 kT (set 5). However, as ϵ_{AW} is decreased from 0.8 to 0.5, the CFD increases above the UCSD because of the influence of Hamaker attraction as the adsorbed amount falls. Two regions of flocculation appear at $\epsilon_{AW} = 0.5$ because at high densities, >0.83, chains are too well-solvated to adsorb significantly. As density is decreased <0.83, the diminished solvent quality causes an increase in adsorption that screens the Hamaker forces. At lower densities, <0.77, flocculation initially occurs because of Hamaker attraction, but an LCST contribution appears at densities below the stabilizer UCSD.

Anchor and Stabilizer Solubility. Set 6 shows the CFD for a chain with a higher P_B^* of 1600, and a lower P_B^* of 1000, equal to that of the solvent. The CFD occurs close to the UCSD and is equal to the CFD for grafted chains with the same P_B^* (set 1). Increasing P_B^* above the solvent value shifts the CFD to higher densities. Because of its high, liquidlike CFD of 0.853, the stabilizer with $P_B^* = 1600$ atm, which is similar to PDMS and PPO, approaches an upper limit on stabilizers useful in supercritical CO_2.

Table 4. Critical Flocculation Densities (CFD) Compared with Experimental Results[a]

A. LFSCF Theory

set no.	r_A	r_B	ν_A	P_A^* (atm)	P_B^* (atm)	ϕ^b	ϵ_{AW}	UCSD	CFD (no Hamaker)	CFD
1	grafted	300	–	–	1600	–	–	0.857	0.855	0.855
	grafted	300	–	–	1200	–	–	0.769	0.762	0.762
	grafted	300	–	–	1000	–	–	0.719	0.71	0.71
	grafted	100	–	–	1200	–	–	0.758	0.758	**
2	75	225	0.25	2300	1200	10^{-5}	3.0	0.766	0.763	0.764
	*					10^{-6}		0.766	0.763	0.764
3	25	275	0.083	2300	1200	10^{-4}	3.0	0.768	0.763	0.763
	10	290	0.033					0.769	0.764	0.766
	5	295	0.017					0.769	0.767	0.780
	0	300	0.000					0.769	none	**
4	75	225	0.25	1900	1200	10^{-4}	3.0	0.766	0.763	0.764
	175	125	0.58					0.758	†	0.766
	200	100	0.67					0.758	†	$\tilde{\rho}<0.77$ (>0.85)
5	75	225	0.25	1900	1200	10^{-4}	6.0	0.766	0.764	0.765
							0.8	0.766	0.765	0.768
							0.5	0.766	0.765	$\tilde{\rho}<0.77$ (>0.83)
6	75	225	0.25	1900	1200	10^{-4}	3.0	0.766	0.763	0.764
		225	0.25		1600			0.854	0.855	0.857
		225	0.25		1000			0.716	0.717	0.718
		125	0.375		1200			0.758	0.762	0.766
		100	0.429		1200			0.758	0.761	0.802
		75	0.50		1200			0.753	0.760	**

B. Experiment (refs 5 and 6)

M_{wA} (10^3)	M_{wB} (10^3)	anchor	stabilizer	ϕ^b	ρ_Θ (g/cm^3)	UCSD (g/cm^3)	CFD (g/cm^3)
4.5	27	PS	PFOA	0.001	0.80	0.79	0.80
7.1	50.3	PVAc	PFOA	0.0027	0.80	0.79	0.79

[a] (*) An empty space indicates no change from the row above; (**) denotes flocculation at all $\tilde{\rho}$; (†) solution not possible at low $\tilde{\rho}$ near UCSD due to high fraction of insoluble anchor.

Stabilizer Length. Set 6 also shows the effect of decreasing the stabilizer length while holding anchor length constant. Similar to the effect of increasing anchor length or decreasing adsorption energy, the CFD rises above the UCSD as stabilizer length decreases because of a failure to screen the Hamaker interactions. At $r_B \leq 75$, flocculation occurs at all densities.

When the Hamaker forces are screened, colloid flocculation occurs near the critical point for the stabilizer in bulk solution, and not at some other volume fraction on the phase diagram. To explain this, consider the stabilizer concentration at the midpoint between the surfaces, ϕ_{int}, in Figure 11a. When the surfaces are far apart ($M = \infty$), ϕ_{int} is at the bulk value of 10^{-4}. However, as the surfaces approach closer, and the stabilizer tails begin to overlap, ϕ_{int} increases significantly, indicated by the solid arrows in Figure 11b. At high pressures, above the critical pressure, the surfaces can approach each other without flocculation, noted by the upper arrow in Figure 11b. However, when the pressure is equal to the critical point pressure for the stabilizer in bulk solution, the surfaces become unstable and flocculate when ϕ_{int} reaches the critical point value (lower arrow in Figure 11b). This description is also supported by analytical scaling and free energy analyses in incompressible solvents.[45]

The LFSCF results are in agreement with stability experiments with PFOA stabilizers in supercritical CO_2.[5,6] As Table 4 shows, stability experiments at the same temperature as our calculations indicate that PEHA emulsions stabilized with PFOA tails flocculate near the Θ density, $\bar{\rho}_\Theta$. For long stabilizer chains, the Θ ($r = \infty$) and actual (finite r) phase boundaries can be very close together and are difficult to distinguish in the experiments already mentioned. In addition, kinetic effects and the definition of flocculation may complicate the experimental location of the exact critical flocculation point. In the LFSCF calculations, however, the flocculation threshold free energy is defined and the phase behavior of the model chains is known exactly. Dispersion polymerization of PMMA in supercritical CO_2 using a grafted PDMS macromonomer stabilizer produces rapidly flocculating particles at pressures below the cloud point for the stabilizer. Uniform, nonflocculated particles are produced at higher pressures, above the cloud point, which is also in agreement with the LFSCF results. Napper[2] has analyzed many studies in *liquid* solvents that suggest a correlation between critical flocculation temperature (or volume, concentration, pressure, etc.) and the Θ point for the infinite molecular weight stabilizer in bulk solution. This observation is contrary to our finding that in supercritical solvents flocculation occurs at the phase boundary for the actual molecular weight of the stabilizer tail. However, the difference between the Θ temperature and the UCST or LCST is often only a few degrees for polymers with $M_w \geq 10^4$ in liquid solvents.

In a previous LFSCF study for end-grafted chains of length $r_c = 50$, the temperature where the second virial coefficient between the surfaces vanished, $T(B = 0)$, was compared with the LCST of the stabilizer tails in bulk solvent.[15] With this method $T(B = 0)$ was consistently less than the LCST. The failure to predict flocculation at the LCST with $T(B = 0)$ may be due to ambiguity in the choice of the lower cutoff distance in the integral for the virial coefficient. The simpler method of defining

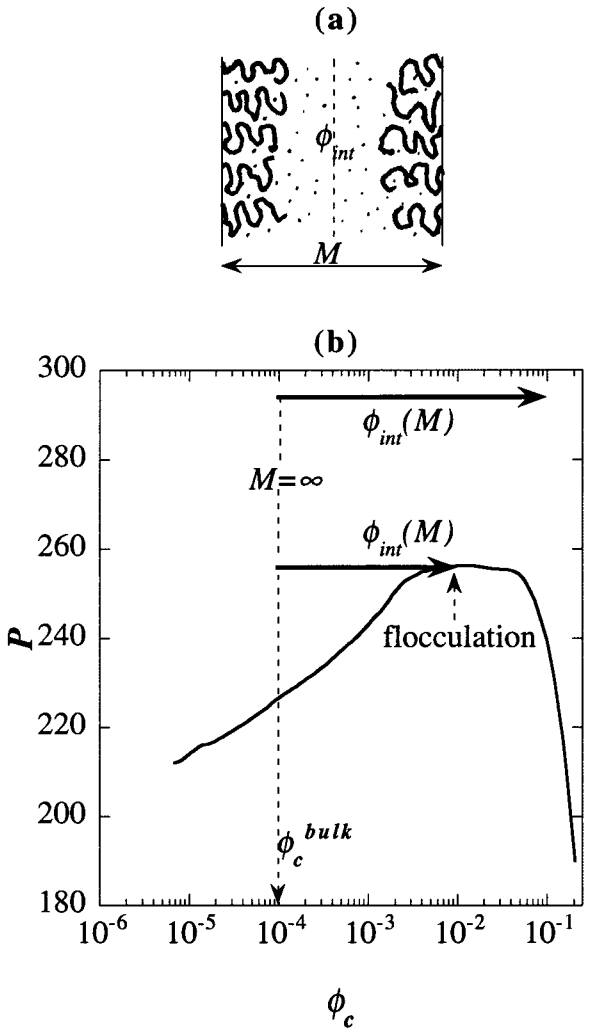

Figure 11. (a) Schematic describing the concentration at the midpoint of the interface. (b) Pressure versus concentration phase diagram describing the correspondence of critical flocculation density (pressure) with the upper critical solution density (critical pressure) for the stabilizer in bulk solution.

the CFD by using a threshold free energy yields a relationship between flocculation and bulk phase behavior that is consistent with experiment.

Conclusions

LFSCF theory predicts that when an adsorbed or grafted layer is thick enough to screen the Hamaker interaction, flocculation occurs at the *critical solution density on the phase boundary of the stabilizer block in bulk solution*. Here, the critical point is for the actual molecular weight of the stabilizer, not the Θ condition at infinite molecular weight. Flocculation at the stabilizer UCSD is driven by the entropy gained by the solvent as it expands away from the adsorbed chains into the bulk solution, analogous to LCST phase separation of bulk polymer solutions. At the UCSD, flocculation occurs because the concentration of stabilizer between the surfaces reaches an unstable value, determined by the bulk solution phase diagram. The correspondence of the CFD and UCSD is in agreement with stability experiments,[5,6] and describes the stabilization of particles produced during dispersion polymerization in supercritical CO_2.[4,9,46,47] In addition, recent Monte Carlo simulations of grafted chains in a supercritical solvent[39] yield the same correspondence between CFD and the stabilizer UCSD in bulk solution.

A block copolymer or end-grafted polymer capable of steric stabilization at densities above the UCSD of the stabilizer tail must have sufficient tail length and adsorbed amount to screen the attractive Hamaker interaction of the dispersed particles. Copolymer properties must be chosen so that tail length and adsorbed amount do not fall below these values, or flocculation will occur above the stabilizer UCSD. Our calculations indicate that flocculation occurs above the UCSD when the adsorption energy per segment is less than $\sim 1\ kT$, but increasing the adsorption energy above this value does not change the CFD significantly.

Chain architecture, represented by either copolymer asymmetry (β) or anchor fraction (ν_A), has a profound effect on layer structure. For the chains in our study, a maximum in adsorbed amount occurs at $\nu_A \approx 0.1$. Flocculation above the UCSD occurs when the fraction of anchor segments deviates too far from this optimum value (e.g., $\nu_A < 0.02$ and $\nu_A > 0.60$). Interestingly, when $\nu_A > 0.3$, the lift-off of anchor segments already described allows more chains to pack on the surface at low densities. Therefore, at densities below the *copolymer* UCSD, copolymers with high anchor fractions ($\nu_A > 0.3$) and shorter tails can create layers just as thick as copolymers with lower anchor fractions.

Changes in anchor solubility, P_A^*, directly affect adsorbed amount, whereas changes in P_B^* directly affect tail extension. High P_A^* and low P_B^* (close to the solvent P_S^*) create the thickest layers at any density, a conclusion supported by results of experiments.[5,22] However, anchor solubility is generally not an issue because most polymers have high P_A^* with respect to CO_2. Rather, it is important that P_A^* match the CED of the dispersed phase, or low adsorption energies will result.[42] Decreasing the solubility of the stabilizer tail, or increasing P_B^*, raises the UCSD, and narrows the range of densities where stabilization is possible.

As solvent density is decreased, grafted layers collapse due to tail−solvent incompatibility, in contrast to adsorbed block copolymer layers, which first collapse but then expand at lower densities, due to increasing adsorption. This collapse-to-expansion transition occurs near the copolymer UCSD in bulk solution, when anchors "lift-off" the surface to allow more copolymer chains to adsorb and escape the increasingly poor solvent. A similar structural transition was observed for homopolymers.[1] This "lift-off" phenomenon may aid stabilization of colloids in supercritical fluids during depressurization to remove the solvent.

Acknowledgment. We thank Isaac C. Sanchez, Mark O'Neill, and Matt Yates for helpful discussions, and acknowledge NSF (CTS-9626828), DOE (DE-FGO3-96ER14664), and the Separations Research Program of the University of Texas. J.C.M. thanks Eastman Chemical Company for providing a graduate fellowship.

Appendix

Reference 15 gives a basic derivation of the LFSCF equations for homopolymers and ref 1 describes the incorporation of adsorption energy. To extend the homopolymer LFSCF theory to copolymers, the summations in refs 1 and 15 are performed over *segment* types, rather than over *molecule* types. This is the same manner in which Evers et al.[16] extended the incompressible homopolymer SCF theory to copolymers. For

example, in the segmental energy, given by

$$u_{A\neq 0}(z) = u'(z) - \sum_B [f_B(z) - f_B^b]P_B^*\nu^* - [\tilde{\rho}(z) - \tilde{\rho}^b]P_A^*\nu^* + \nu^* kT \sum_B [\langle f_B(z)\rangle - f_A^b]\chi_{AB} \quad \text{(A1)}$$

the summations are performed over all segment types B, which includes anchor (A), stabilizer (B), solvent (s), and holes (o). The connectivity of the copolymer is reflected in the chain probabilities using the recursive propagation algorithms

$$G_A(z,s|1) = \lambda_1 G_A(z-1, s-1|1) + \lambda_0 G_A(z, s-1|1) + \lambda_1 G_A(z+1, s-1|1) \quad \text{(A2)}$$

$$G_B(z,s|r_c) = \lambda_1 G_B(z-1, s+1|r_c) + \lambda_0 G_B(z, s+1|r_c) + \lambda_1 G_B(z+1, s+1|r_c) \quad \text{(A3)}$$

The index is switched from A to B at segment $s = r_A + 1$ in eq A2 (forward propagation) and from B to A in eq A3 at $s = r_A$ in eq A3 (backwards propagation). The chain segment probabilities, $G_A(z,s|r_A)$ and other quantities in eqs A2 and A3 have their usual definitions.[15,16]

Because the lattice fluid equation of state for bulk solutions is generally presented for homopolymers,[19] a mixing rule describes the energy parameter for the copolymer solutions and is given by

$$\epsilon^* = \sum_A \epsilon_A^* + \sum_A \sum_{B\neq A} \phi_A\phi_B\chi_{AB}kT \quad \text{(A4)}$$

The equation of state and chemical potential expressions are as given in ref 19, except that for the copolymer solution, $T^* = \epsilon^*/k$ and $P^* = \epsilon^*/\nu^*$, with ϵ^* given by eq A4.

References and Notes

(1) Meredith, J. C.; Johnston, K. P. *Macromolecules* **1998**, *31*, 5507−5517.
(2) Napper, D. H. *Polymeric Stabilization of Colloidal Dispersions*; Academic: London, 1983.
(3) Canelas, D. A.; Betts, D. E.; DeSimone, J. M. *Macromolecules* **1996**, *29*, 2818−2821.
(4) Guan, Z.; DeSimone, J. M. *Macromolecules* **1994**, *27*, 5527−5532.
(5) O'Neill, M. L.; Yates, M. Z.; Johnston, K. P.; Wilkinson, S. P.; Canelas, D. A.; Betts, D. E.; DeSimone, J. M. *Macromolecules* **1997**, *30*, 5050−5059.
(6) Yates, M. Z.; O'Neill, M. L.; Johnston, K. P.; Webber, S.; Canales, D. A.; Betts, D. A.; DeSimone, J. M. *Macromolecules* **1997**, *30*, 5060−5067.
(7) Mawson, S.; Johnston, K. P.; DeSimone, J. M.; Betts, D. E.; McClain, J. B. *Macromolecules* **1997**, *30*, 71.
(8) Mawson, S.; Yates, M. Z.; O'Neill, M. L.; Johnston, K. P. *Langmuir* **1997**, *13*, 1519−1528.
(9) O'Neill, M. L.; Yates, M. Z.; Johnston, K. P.; Smith, C. D.; Wilkinson, S. P. *Macromolecules* **1998**, *31*, 2838−2847.
(10) O'Neill, M. L.; Yates, M. Z.; Johnston, K. P.; Smith, C. D.; Wilkinson, S. P. *Macromolecules* **1998**, *31*, 2848−2856.
(11) Marques, C.; Joanny, J. F.; Leibler, L. *Macromolecules* **1988**, *21*, 1051−1059.
(12) Tirrell, M. In *Solvents and Self-Organization of Polymers*; Webber, S. E., et al., Eds.; Kluwer Academic: Dordrecht, 1996; Vol. 327, pp 281−308.
(13) Szleifer, I.; Carignano, M. A. *Adv. Chem. Phys.* **1996**, *94*, 165−260.
(14) Grest, G. S.; Murat, M. In *Monte Carlo and Molecular Dynamics Simulations in Polymer Science*; Binder, K., Ed.; Oxford University: New York, 1995.
(15) Peck, D. G.; Johnston, K. P. *Macromolecules* **1993**, *26*, 1537−1545.
(16) Evers, O. A.; Scheutjens, J. M. H. M.; Fleer, G. J. *Macromolecules* **1990**, *23*, 5221−5233.
(17) Fleer, G. J.; Cohen Stuart, M. A.; Schuetjens, J. M. H. M.; Cosgrove, T.; Vincent, B. In *Polymers at Interfaces*; Chapman and Hall: London, 1993; p 282.
(18) Sanchez, I. C. In *Encyclopedia of Physical Science and Technology*; Academic: New York, 1987; Vol. XI, pp 1−18.
(19) Sanchez, I. C.; Panayiotou, C. G. In *Models for Thermodynamic and Phase Equilibria Calculations*; Sandler, S., Ed.; Dekker: New York, 1993; Vol. 52, pp 187−285.
(20) Evers, O. A.; Scheutjens, J. M. H. M.; Fleer, G. J. *Macromolecules* **1991**, *24*, 5558−5566.
(21) Barton, A. F. M. In *CRC Handbook of Solubility Parameters and other Cohesion Parameters*; CRC: Boca Raton, FL, 1983; pp 425−429.
(22) O'Neill, M. L.; Cao, Q.; Fang, M.; Johnston, K. P.; Wilkinson, S. P.; Smith, C. D.; Kerschner, J. L.; Jureller, S. H. *Ind. Eng. Chem. Res.* **1998**, in press.
(23) Scheutjens, J. M. H. M.; Fleer, G. J. *Macromolecules* **1985**, *18*, 1882−1900.
(24) Munch, M.; Gast, A. P. *Macromolecules* **1988**, *21*, 1360−1366.
(25) Munch, M.; Gast, A. P. *Macromolecules* **1988**, *21*, 1366−1372.
(26) Sanchez, I. C. L., R. H. *Macromolecules* **1978**, *11*, 1145−1156.
(27) Luna-barcenas, G.; Meredith, J. C.; Gromov, D. G.; Sanchez, I. C.; de Pablo, J. J.; Johnston, K. P. *J. Chem. Phys.* **1997**, *107*, 1−11.
(28) Flory, P. J. *Principles of Polymer Chemistry*; Cornell University: New York, 1953.
(29) DiMarzio, E. A. *J. Chem. Phys.* **1965**, *42*, 2101−2106.
(30) Grest, G. S.; Murat, M. *Macromolecules* **1993**, *26*, 3108−3117.
(31) Soga, K. G.; Guo, H.; Zuckerman, M. J. *Europhys. Lett.* **1995**, *29*, 531−536.
(32) deGennes, P. G. *Macromolecules* **1980**, *13*, 1069−1075.
(33) Alexander, S. *J. Phys. Paris* **1977**, *38*, 983−987.
(34) Milner, S. T.; Witten, T. A.; Cates, M. E. *Macromolecules* **1988**, *21*, 2610−2619.
(35) Zhulina, E. B.; Borisov, O. V.; Pryamitsyn, V. A.; Birshtein, T. M. *Macromolecules* **1991**, *24*, 140−149.
(36) Israelachvili, J.; Tirrell, M. *Proc. Natl. Acad. Sci. U.S.A.* **1987**, *84*, 4733−4736.
(37) Auroy, P.; Auvray, L.; Leger, L. *Macromolecules* **1991**, *24*, 2523−2528.
(38) Kent, M. S.; Lee, L.-T.; Farnoux, B.; Rondelez, F. *Macromolecules* **1992**, *25*, 6240−6247.
(39) Meredith, J. C.; Sanchez, I. C.; Johnston, K. P.; de Pablo, J. J. *J. Chem. Phys.* **1998**, in press.
(40) Baranowski, R.; Whitmore, M. D. *J. Chem. Phys.* **1995**, *103*, 2343−2353.
(41) Harrison, K. L.; da Rocha, S. R. P.; Yates, M. Z.; Johnston, K. P.; Canelas, D. A.; DeSimone, J. M. submitted for publication in *Langmuir*.
(42) Harrison, K. L.; Johnston, K. P.; Sanchez, I. C. *Langmuir* **1996**, *12*, 2637−2644.
(43) de Gennes, P. G. *Adv. Colloid Interface Sci.* **1987**, *27*, 189−209.
(44) Parsonage, E.; Tirrell, M.; Watanabe, H.; Nuzzo, R. G. *Macromolecules* **1991**, *24*, 1987−1995.
(45) Klein, J.; Pincus, P. *Macromolecules* **1982**, *15*, 1129−1135.
(46) DeSimone, J. M.; Maury, E. E.; Menceloglu, Y. Z.; McClain, J. B.; Romack, T. J.; Combes, J. R. *Science* **1994**, *265*, 356−359.
(47) Shaffer, K. A.; Jones, T. A.; Canelas, D. A.; DeSimone, J. M.; Wilkinson, S. P. *Macromolecules* **1996**, *29*, 2704−2706.
(48) Lai, C.-C.; Tan, C.-S. *Fluid Phase Equilib.* **1995**, *111*, 127−141.
(49) Killmann, E.; Korn, M.; Bergmann, M. In *Adsorption from Solution*; Ottewill, R. H., Rochester, C. H., Smith, A. L., Eds.; Academic: London, 1982; pp 259−272.

MA980260P